

Hidden vortices in a Bose-Einstein condensate in a rotating double-well potentialLinghua Wen (文灵华),^{1,2} Hongwei Xiong (熊宏伟),³ and Biao Wu (吴飙)⁴¹*Institute of Physics, Chinese Academy of Sciences, Beijing 100190, China*²*Department of Physics, Liaocheng University, Shandong 252059, China*³*State Key Laboratory of Magnetic Resonance and Atomic and Molecular Physics, Wuhan Institute of Physics and Mathematics, Chinese Academy of Sciences, Wuhan 430071, China*⁴*International Center for Quantum Materials, Peking University, Beijing 100871, China*

(Received 11 February 2010; published 24 November 2010)

We study vortex formation in a Bose-Einstein condensate in a rotating double-well potential. In addition to the ordinary quantized vortices and elusive ghost vortices, “hidden” vortices are found distributed along the central barrier. These hidden vortices are invisible like ghost vortices but carry angular momentum. Moreover, their core size is not given by the healing length, but is strongly influenced by the external potential. We find that the Feynman rule can be well satisfied only after including the hidden vortices. There is no critical rotation frequency for the formation of hidden vortices while there is one for the formation of ordinary visible vortices. Hidden vortices can be revealed in the free expansion of Bose-Einstein condensates. In addition, the hidden vortices in a Bose-Einstein condensate can appear in other external potentials, such as a rotating anisotropic toroidal trap.

DOI: [10.1103/PhysRevA.82.053627](https://doi.org/10.1103/PhysRevA.82.053627)

PACS number(s): 03.75.Lm, 03.75.Kk, 67.85.De

I. INTRODUCTION

The double-well (DW) potential is an important model potential for its simplicity and yet richness in physics. The properties of Bose-Einstein condensates (BECs) in a DW potential have been studied extensively since the realization of BECs [1]. With the advances of technology, DW potentials for ultracold atoms can now be realized in experiments with great controllability and precision [2–4]. One particular interesting development is the possibility of rotating a DW potential via radiofrequency dressing [5]. This opens the door to a study of the behavior of vortices in a degenerate quantum gas in a rotating DW potential. As topological defects, quantized vortices have contributed greatly to revealing the phase coherence, superfluidity, and nonlinear phenomena in degenerate quantum gases, and have been the subject of extensive experimental and theoretical studies [6–23].

The DW potential also offers a unique testing ground for the well-known Feynman rule of vortices [24]. The Feynman rule is a very powerful relation that links the total number of vortices with the angular frequency of rotation. Feynman argued that for a rotating superfluid with angular frequency Ω , the superfluid should be regarded as a classical fluid when it reaches the steady state. This leads to the important mathematical relation that the total number of vortices N_v in an area A is linearly proportional to Ω , $2\pi\hbar N_v/m = 2\Omega A$. Alternatively, the Feynman rule can be expressed as $l_z/\hbar = N_v/2$ with l_z being the mean angular momentum per atom at equilibrium [14,15,24,25]. This rule was formulated originally for uniform superfluid helium, and has been intensively studied both theoretically [25,26] and experimentally [9,10] for a BEC trapped in a single harmonic potential. It is interesting to know how the rule fares in a more complicated geometric confinement. The DW potential provides a clear opportunity to answer this question.

In this paper we describe a comprehensive two-dimensional (2D) numerical study of vortex formation in a BEC in a rotating DW potential. We find, surprisingly, that the *in situ* density distribution seems to violate the Feynman rule

significantly in that the total number of vortices with visible cores is significantly smaller than $2l_z/\hbar$. With the belief that the Feynman rule should hold in some form, we carefully analyze the results and find that these “missing” vortices are distributed along the central barrier of the DW potential. Unlike the usual vortex, these vortices have no visible cores but have phase singularities, and their core size is not given by the healing length but is strongly influenced by the external potential. For this reason, they may be called “hidden vortices.” With the inclusion of the hidden vortices, one recovers the Feynman rule.

These hidden vortices remind us of the ghost vortices found numerically in Ref. [25]. In general, for the case of a simply connected trap the ghost vortices lie at the outskirts of the condensate and for the case of multiply connected trap the ghost vortices are in the outer region of the cloud, where the particle density $|\psi|^2$ is very small. As a result, like hidden vortices, they show up in numerical results as phase singularities but have no visible cores. However, there are key differences: the ghost vortex carries no angular momentum while the hidden vortex does; the core size of the ghost vortex is determined by the healing length as for the usual visible vortex while that of the hidden vortex is determined by the shape of the external potential. In addition, we find that with increasing rotation frequency Ω the hidden vortices appear first in the DW system, followed by ghost vortices and the usual visible vortices. Furthermore, angular momentum can be put gradually into the BEC via the generation of hidden vortices while the emergence of a visible vortex is still accompanied by a jump in the system’s angular momentum. Although the hidden vortices are invisible in the *in situ* density distribution, after free expansion of the BEC, they can appear in the density distribution because of their stable topological structure.

It is well known that there exists a special type of vortex called a Josephson vortex (or fluxon) in a long superconducting Josephson junction [27] or between two weakly coupled BECs [28,29]. These Josephson vortices can be regarded as hidden vortices. However, the hidden vortex is a more general notion than the Josephson vortex (fluxon) as a hidden vortex can exist

in a non-DW potential (or non-Josephson structure). We have used a rotating anisotropic toroidal trap to illustrate this point.

This paper is organized as follows. In Sec. II, we present a phenomenological model to describe the dynamics of a BEC confined in a rotating DW potential in the presence of dissipation. Hidden vortices are found in the rotating DW BEC, where the Feynman rule is satisfied only after inclusion of these hidden vortices. A simple and feasible scheme is proposed to observe the hidden vortices. In Sec. III, we study the vortex formation process and the critical rotation frequency in the rotating DW BEC. In Sec. IV, we discuss the hidden vortices in a BEC confined in a rotating anisotropic toroidal trap. Section V provides a summary and discussion.

II. HIDDEN VORTICES IN A ROTATING DW BEC AND FEYNMAN RULE

We consider the situation where the condensate is tightly confined in the axial direction ($\omega_x, \omega_y \ll \omega_z$) so that the system is effectively two dimensional. The DW potential is described by

$$V_{\text{DW}}(x, y) = \frac{x^2 + \lambda^2 y^2}{4} + V_0 e^{-x^2/2\sigma^2}, \quad (1)$$

where V_0 and σ are the height and width of the potential barrier, respectively, and $\lambda = \omega_y/\omega_x$ denotes the anisotropy parameter of the harmonic trap. In the presence of dissipation, the order parameter in the frame rotating with the angular velocity Ω around the z axis obeys the time-dependent Gross-Pitaevskii equation

$$(i - \gamma) \frac{\partial \psi}{\partial t} = [-(\nabla_x^2 + \nabla_y^2) + V_{\text{DW}} + c|\psi|^2 - \Omega L_z] \psi. \quad (2)$$

Here $L_z = i(y\partial_x - x\partial_y)$ is the z component of the angular-momentum operator, γ characterizes the degree of dissipation, and c is the 2D interatomic interaction strength. In this work, length, time, energy, angular momentum, and rotation angular frequency are in units of $d_0 = \sqrt{\hbar/2m\omega_x}$, $1/\omega_x$, $\hbar\omega_x$, \hbar , and ω_x , respectively. The phenomenological dissipation model (2) is a variation of that in Ref. [25]. For the case of a BEC in a rotating harmonic trap, our computation results agree well with the experimental observations in Ref. [8] and the simulation results in Ref. [25].

In our calculations, we first obtain the initial ground-state order parameter in the DW potential by the imaginary time propagation method [30–32] for $\Omega = 0$. The vortex formation process is then studied by solving Eq. (2) numerically with different Ω . Here we consider a BEC of ^{87}Rb atoms with repulsive interaction. The system parameters are chosen to be $\omega_x = \omega_y = 2\pi \times 40$ Hz, $\omega_z = 2\pi \times 800$ Hz, $V_0 = 40$, $\sigma = 0.5$, $c = 600$. In Eq. (2), variation of the nonzero γ only influences the relaxation time scale but does not change the dynamics of vortex formation and the ultimate steady vortex structure. In our computation, we choose $\gamma = 0.03$, which corresponds to a temperature of about $0.1T_c$ [33].

Figure 1(a) shows the steady density distribution $|\psi|^2$ at $t = 250$ for a DW potential rotating with $\Omega = 0.9$. From this *in situ* density distribution, we see a pair of ordinary vortex lattices with triangular structure as expected from the rotating DW configuration. However, by simply counting, we find

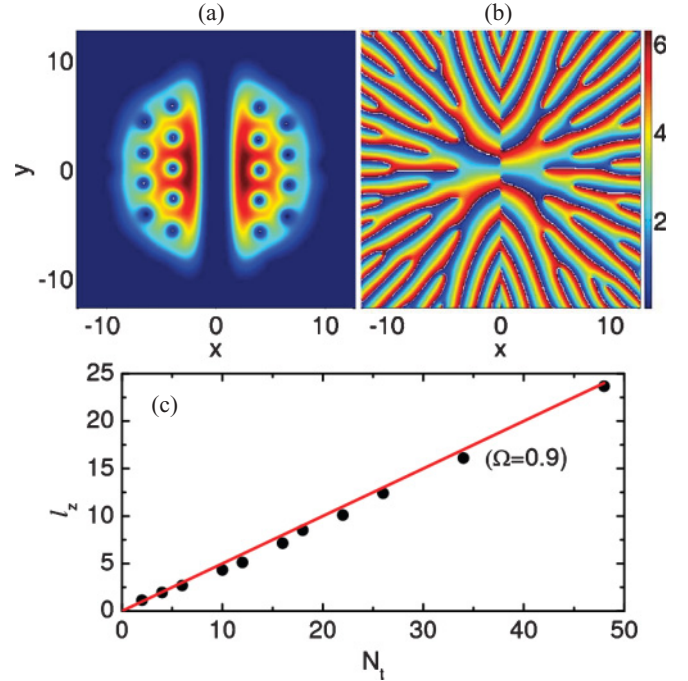


FIG. 1. (Color online) (a) Density distribution $|\psi|^2$ and (b) phase distribution of ψ at $t = 250$ after rotating the system with $\Omega = 0.9$. (c) l_z versus $N_t/2$ for different Ω , where the line is $l_z = N_t/2 = (N_v + N_h)/2$ and the solid circles denote the numerical results. The value of the phase varies continuously from 0 to 2π . The darker color area indicates lower density or phase. The small deviation between the line and the circles in (c) may be due to the inhomogeneous condensate density [25]. Here x and y are in units of d_0 , l_z is in units of \hbar , and Ω is in units of ω_x .

something surprising. In Fig. 1(a), the total number of vortices is $N_v = 18$. Numerical results show that the mean angular momentum per atom $l_z = \iint \psi^* L_z \psi dx dy / \iint |\psi|^2 dx dy$ is about $l_z \approx 16 \gg N_v/2$. It seems that the Feynman rule [14,15,24,25] is no longer satisfied. For other rotation frequencies, this seemingly significant violation of Feynman rule is also found. With the belief that the Feynman rule should always hold, this violation indicates that some angular momentum is missing and is not manifested in the form of ordinary vortices.

To find the missing angular momentum, we look into the phase distribution of $\psi(x, y, t = 250)$, which is plotted in Fig. 1(b). We find that in addition to the phase singularities corresponding to the above mentioned vortices, there are other phase defects, distributed along the central barrier and the outskirts of the cloud. The initial reaction is that these phase defects, which are invisible in the *in situ* density distribution, are ghost vortices as discussed in Ref. [25]. Since ghost vortices are known not to carry angular momentum, it seems that these invisible phase defects cannot account for the missing angular momentum. However, a more careful examination shows otherwise.

The phase singularities along the central barrier are not ghost vortices and they carry angular momentum. To see this, we assume N_h is the total number of phase singularities along the central barrier, and $N_t = (N_v + N_h)$ is the sum of N_v and N_h . From Fig. 1(b), we have $N_h = 16$. If we include these, the Feynman rule $l_z \simeq N_t/2 = (N_v + N_h)/2$ is well satisfied,

indicating that these phase singularities do carry angular momentum like the usual visible vortices. We have checked other rotation frequencies and found that the Feynman rule can always be well satisfied by including the phase defects along the central barrier. In Fig. 1(c), we have plotted the dependence of l_z on $N_t/2$ for different rotation angular frequencies. The solid line is the Feynman rule $l_z = N_t/2$ while the solid circles are the numerical results for l_z at equilibrium. The excellent agreement between them strongly supports that phase singularities along the central barrier carry angular momentum, and thus are not ghost vortices. We call these topological defects along the central barrier hidden vortices because of their difference from the ordinary vortex and the ghost vortex.

Two factors are involved in why a hidden vortex carries angular momentum while a ghost vortex does not: location and core size. To see this, we consider a phase defect with a singly quantized circulation in the condensate. The angular momentum carried by this phase defect varies with the location as $l_z \sim (1 - r^2/R^2)$ [14], where R is the size of the condensate and r is the distance from the center. Since a ghost vortex always lies on the outer region of the condensate, meaning $r \sim R$, its contribution to angular momentum is negligible. For a hidden vortex, which is located near the center of the condensate, we have $r < R$. Therefore, its contribution to the angular momentum is significant and needs to be counted for the Feynman rule. Furthermore, the core size of a nonhidden vortex is about the healing length $\xi = \sqrt{1/nc}$ (n is the local density of the condensate without vortices). Since n is very small for a ghost vortex, the core size of a ghost vortex approaches an infinite value. As a result, ghost vortices contribute to neither the angular momentum nor the energy of the system. For a hidden vortex, n is also very small at its location. However, its core size is determined by the barrier width, not the healing length. Therefore, a hidden vortex can contribute to the angular momentum. With the local density approximation, our numerical calculations do show that the hidden vortices carry significant angular momentum while the angular momentum due to a ghost vortex can be neglected.

Even though the hidden vortices are invisible in the *in situ* density distribution as shown in Fig. 1(a), we find numerically that they show up in the cloud after free expansion (see the following discussion). This makes it possible to observe and test the existence of these hidden vortices experimentally.

We use the state shown in Figs. 1(a) and 1(b) as an example. After a short expansion time, the state begins to look very different. In Fig. 2, the density distribution and phase distribution at the expansion time $\tau = 4$ are plotted. We see clearly in Figs. 2(a) and 2(b) that, in addition to 18 vortices already shown in the *in situ* density distribution [see Fig. 1(a)], a series of new ordinary vortices appear along the symmetric axis of the two condensates. These new visible vortices originate physically from the hidden vortices. It is not difficult to understand the revelation of the hidden vortices during the free expansion. The core of a vortex (hidden, ghost, or visible) is also a velocity singularity, where the velocity approaches infinity. Because the kinetic energy should be finite, during free expansion where the angular momentum is conserved, no atoms will be allowed into the core area. As a result, the core is stable and will not be destroyed. At the same time, as the two BECs begin to overlap, atoms begin to move into the

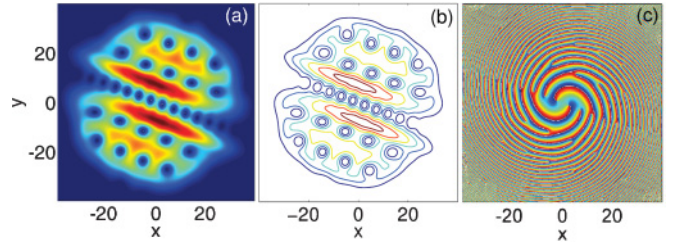


FIG. 2. (Color online) (a) Density distribution, (b) density contour, and (c) phase distribution after the cloud expands freely for $\tau = 4$. Before the free expansion, the system has rotated with $\Omega = 0.9$ for $t = 250$. The darker color area or contour indicates lower density or phase. Here x and y are in units of d_0 .

central region and fill the space between hidden vortex cores, rendering them visible. Not all hidden vortices can be revealed during free expansion. As shown in Fig. 2(c), there still exist several remnant hidden vortices along the boundary between the two flows, which is due to the strong repulsion and pushing of the newly formed visible vortices during the expansion.

Because the ghost vortices lie on the outskirts, the locations of their phase defects move outward during the free expansion. Consequently, the density in the regime of the ghost vortices is always negligible. This is the reason that the ghost vortices will not become visible vortices during the expansion.

III. VORTEX FORMATION PROCESS AND CRITICAL ROTATION FREQUENCY FOR A ROTATING DW BEC

The vortex formation process with the rotating DW potential is very different from that with a single harmonic potential. There is a critical angular frequency for a rotating single-well potential to create vortices: when the angular frequency Ω is below the critical angular frequency, only ghost vortices are formed at the outskirts of the BEC cloud and the cloud does not carry any significant angular momentum; when Ω is larger than the critical frequency, visible vortices begin to appear along with a jump in the angular momentum [25]. For the rotating DW system, the vortex formation starts with a pair of hidden vortices. As seen in Figs. 3(a)–3(e), the hidden vortex pair begin their formation at the ends of the potential barrier, then move toward the center. This is followed by a sequence of other hidden vortex pairs. Ghost vortices begin to appear only after several pairs of hidden vortices are already formed. Eventually at the critical rotation frequency $\Omega_c = 0.59$, a pair of ordinary visible vortices are formed [see Fig. 3(f)], accompanied by a jump in the system's angular momentum [see Fig. 3(g)].

The dependence of the angular momentum per atom, l_z , on the rotation frequency Ω is shown in Fig. 3(g). It is clear from the figure that the angular momentum l_z increases gradually and continuously with Ω until a jump occurs at $\Omega_c = 0.59$. Along with Figs. 3(a)–3(e), this shows that the hidden vortices can gradually increase the system's angular momentum as they move toward the center. The ghost vortex has no capacity to carry angular momentum. As demonstrated clearly in Figs. 3(d) and 3(e), even as a pair of ghost vortices move toward the center and eventually become a pair of ordinary visible vortices, the change in the angular momentum is very sudden as witnessed by the jump in Fig. 3(g).

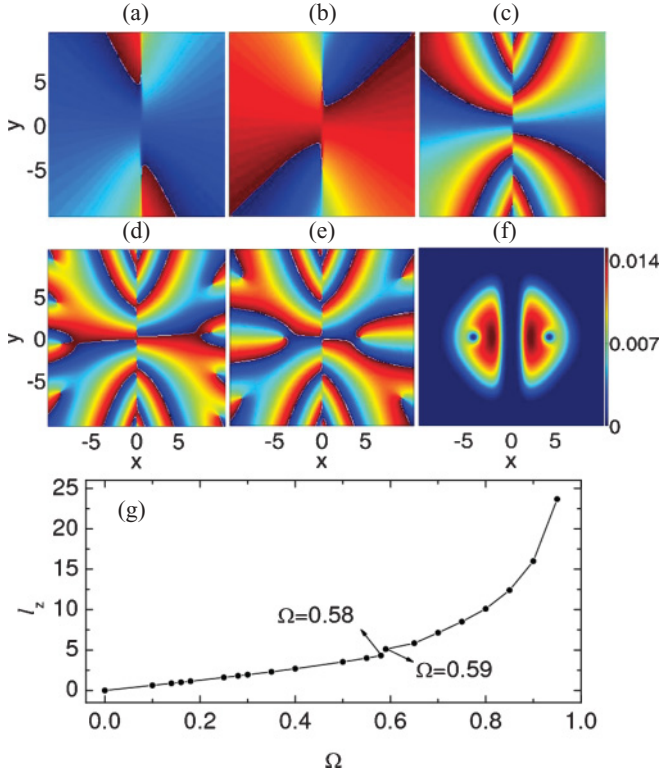


FIG. 3. (Color online) Phase distributions of ψ at $t = 250$ for different rotation frequencies: (a) $\Omega = 0.1$; (b) $\Omega = 0.12$; (c) $\Omega = 0.5$; (d) $\Omega = 0.58$; (e) $\Omega = 0.59$. (f) The density distribution $|\psi|^2$ at $t = 250$ for $\Omega = 0.59$. (g) Angular momentum per atom l_z versus Ω . The darker color area indicates lower phase or density. Here x and y are in units of d_0 , l_z is in units of \hbar , and Ω is in units of ω_x .

By virtue of the data fit, another interesting feature in Fig. 3(g) is that, for $\Omega < \Omega_c$, l_z increases linearly; in contrast, for $\Omega \geq \Omega_c$, l_z grows exponentially. These two different regimes marked by linear and perfectly exponential growth are likely associated with the fact that the hidden vortices only form along the central barrier but the ordinary visible vortices can emerge in the whole region of the cloud.

IV. HIDDEN VORTICES IN A BEC CONFINED IN A ROTATING TOROIDAL TRAP

Hidden vortices can exist in non-DW potentials. To illustrate this point, we consider a BEC confined in a rotating toroidal trap. The toroidal trap is given by

$$V_{\text{TT}}(x, y) = \frac{x^2 + y^2}{4} + V_0 e^{-(\alpha x^2 + y^2/\alpha)/2\sigma^2}, \quad (3)$$

where α characterizes the anisotropy of the 2D central barrier in the toroidal trap. $\alpha = 1$ corresponds to a circular toroidal trap, which has recently been studied by Aftalion *et al.* [34]. In addition, Piazza *et al.* [23] investigated the vortex-induced phase-slip dissipation in an isotropic toroidal BEC flowing through a barrier. We focus on an anisotropic (deformed) toroidal trap ($\alpha \neq 1$), where the lack of rotation symmetry excludes the possibility of formation of a multi-quantized vortex (giant vortex) in the center of the trap for sufficiently large rotation frequency Ω and sufficiently narrow barrier. The

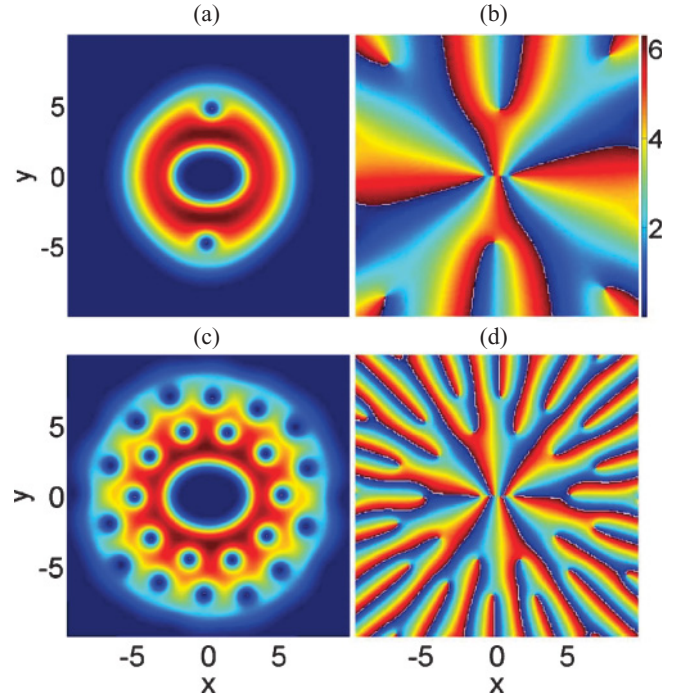


FIG. 4. (Color online) Density distributions $|\psi|^2$ (left) and phase distributions of ψ (right) at $t = 250$ for a toroidal trap rotating with $\Omega = 0.6$ (top) and $\Omega = 0.9$ (bottom). The corresponding parameters are $V_0 = 40$, $\alpha = 0.8$, $\sigma = 1$, $\gamma = 0.03$, and $c = 600$. The value of the phase varies continuously from 0 to 2π . The darker color area indicates lower density or phase. Here x and y are in units of d_0 .

numerical procedure for this toroidal trap is identical to the DW potential. In Fig. 4 we display the steady density distributions $|\psi|^2$ (left) and the corresponding phase distributions of ψ (right) at $t = 250$ for an anisotropic toroidal trap rotating with $\Omega = 0.6$ (top) and $\Omega = 0.9$ (bottom). The parameters are $V_0 = 40$, $\alpha = 0.8$, $\sigma = 1$, $\gamma = 0.03$, and $c = 600$.

At $\Omega = 0.6$, two visible vortices appear in the *in situ* density distribution as shown in Fig. 4(a). Moreover, there is an ellipsoidal density hole in the trap center which looks like a giant vortex. In the phase distribution displayed in Fig. 4(b), we see that as well as two phase singularities corresponding to the two visible vortices, there are other phase defects, which are distributed along the long axis of the central barrier and at the outskirts of the cloud. The four singly quantized phase defects along the long axis of the central barrier show that the ellipsoidal density hole is not a giant vortex. Our numerical simulation further indicates that the four single-quantized phase defects carry angular momentum and satisfy the Feynman rule together with the two visible vortices. Therefore, they are four singly quantized hidden vortices. On the other hand, the phase defects at the outskirts of the cloud are ghost vortices because they contribute no angular momentum to the system.

With increase of the rotation frequency, more vortices nucleate and a triangular vortex lattice forms eventually [see Fig. 4(c)]. At the same time, as shown in Fig. 4(d), more hidden vortices also show up in the central barrier region, e.g., there are six hidden vortices for $\Omega = 0.9$. However, these hidden vortices do not form a triangular lattice, and they are still

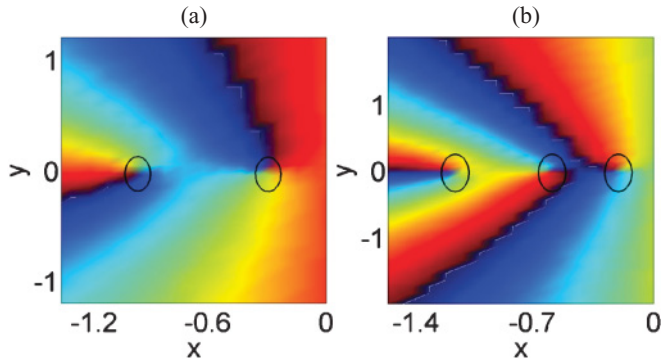


FIG. 5. (Color online) Local enlargement of (a) Fig. 4(b) and (b) Fig. 4(d), where the circles mark the positions of hidden vortices. Here x and y are in units of d_0 .

distributed along the long axis of the ellipsoidal central barrier. This shows from another perspective that the hidden vortex is different from the usual visible vortex. Local enlargements of Figs. 4(b) and 4(d) are given in Fig. 5, where the circles denote the positions of hidden vortices.

Note that in our simulation we did not observe the generation of vortex-antivortex pairs in the double-well case and the toroidal trap, as were reported, respectively, in Ref. [35] and Ref. [23]. For the double-well case, it is because there was no free expansion in Ref. [35] so that the extra energy caused by removing the central barrier is used to create vortex-antivortex pairs. In the toroidal trap, the vortex-antivortex pairs seen in Ref. [23] are suppressed by the dissipation term in our simulation.

V. DISCUSSION AND SUMMARY

In summary, we have investigated numerically the formation of vortices in a rotating double-well potential. We found that, other than the usual visible and ghost vortices, there exists

another type of vortex, which we call a hidden vortex. Unlike the usual visible vortex, these hidden vortices are invisible in the *in situ* density distribution. They differ also from the ghost vortex by being able to carry angular momentum. In addition, the core size of the hidden vortex is not given by the healing length and is strongly influenced by the shape of the external potential. Only after inclusion of the hidden vortices can the Feynman rule be satisfied.

The hidden vortex has appeared in the literature under other names. Examples are the magnetic fluxons in a superconducting long Josephson junction in a parallel magnetic field [27], Josephson vortices between two long parallel coupled atomic BECs [28], and rotational fluxons of BECs in rotating coplanar double-ring traps [29]. The giant vortices (sometimes called “phantom vortices”) in a cylindrical hard-walled bucket or a quadratic plus quartic trap [36] or a circular toroidal trap [34] can also be regarded as a form of hidden vortex. However, as we have illustrated in the preceding section with an anisotropic toroidal trap, hidden vortices can occur in many settings other than the previously mentioned structure or potentials. Therefore, the hidden vortex is a more general notion that encompass all the essential features of the Josephson and giant vortices. At the same time, these names, such as the Josephson vortex and giant vortex, each coined for a special potential, show that it is necessary to distinguish the hidden vortex from the usual visible vortex and the ghost vortex.

ACKNOWLEDGMENTS

We thank B. L. Lv, K. J. Jiang, Y. P. Zhang, and L. Mao for helpful discussions. This work was supported by NSFC (Grants No. 10825417, No. 10875165, and No. 10847143), NKBRFS of China (Grant No. 2011CB921503), NSF of Shandong Province (Grant No. Q2007A01), and the Ph.D. Foundation of Liaocheng University.

-
- [1] A. Smerzi, S. Fantoni, S. Giovanazzi, and S. R. Shenoy, *Phys. Rev. Lett.* **79**, 4950 (1997); G. J. Milburn, J. Corney, E. M. Wright, and D. F. Walls, *Phys. Rev. A* **55**, 4318 (1997).
 - [2] M. Albiez, R. Gati, J. Fölling, S. Hunsmann, M. Cristiani, and M. K. Oberthaler, *Phys. Rev. Lett.* **95**, 010402 (2005).
 - [3] S. Hofferberth, I. Lesanovsky, B. Fischer, T. Schumm, and J. Schmiedmayer, *Nature (London)* **449**, 324 (2007); B. V. Hall, S. Whitlock, R. Anderson, P. Hannaford, and A. I. Sidorov, *Phys. Rev. Lett.* **98**, 030402 (2007); G. B. Jo, Y. Shin, S. Will, T. A. Pasquini, M. Saba, W. Ketterle, D. E. Pritchard, M. Vengalattore, and M. Prentiss, *ibid.* **98**, 030407 (2007).
 - [4] J. Estève, C. Gross, A. Weller, S. Giovanazzi, and M. K. Oberthaler, *Nature (London)* **455**, 1216 (2008); A. Weller, J. P. Ronzheimer, C. Gross, J. Esteve, M. K. Oberthaler, D. J. Frantzeskakis, G. Theocharis, and P. G. Kevrekidis, *Phys. Rev. Lett.* **101**, 130401 (2008).
 - [5] S. Hofferberth, I. Lesanovsky, B. Fischer, J. Verdu, and J. Schmiedmayer, *Nature Phys.* **2**, 710 (2006).
 - [6] Y. J. Lin, R. L. Compton, A. R. Perry, W. D. Phillips, J. V. Porto, and J. B. Spielman, *Phys. Rev. Lett.* **102**, 130401 (2009).
 - [7] I. B. Spielman, *Phys. Rev. A* **79**, 063613 (2009).
 - [8] K. W. Madison, F. Chevy, W. Wohlleben, and J. Dalibard, *Phys. Rev. Lett.* **84**, 806 (2000); K. W. Madison, F. Chevy, V. Bretin, and J. Dalibard, *ibid.* **86**, 4443 (2001).
 - [9] J. R. Abo-Shaeer, C. Raman, J. M. Vogels, and W. Ketterle, *Science* **292**, 476 (2001).
 - [10] P. C. Haljan, I. Coddington, P. Engels, and E. A. Cornell, *Phys. Rev. Lett.* **87**, 210403 (2001).
 - [11] E. Hodby, G. Hechenblaikner, S. A. Hopkins, O. M. Marago, and C. J. Foot, *Phys. Rev. Lett.* **88**, 010405 (2001).
 - [12] M. W. Zwierlein, J. R. Abo-Shaeer, A. Schirotzek, C. H. Schunck, and W. Ketterle, *Nature (London)* **435**, 1047 (2005).
 - [13] C. N. Weiler, T. W. Neely, D. R. Scherer, A. S. Bradley, M. J. Davis, and B. P. Anderson, *Nature (London)* **455**, 948 (2008); K. C. Wright, L. S. Leslie, A. Hansen, and N. P. Bigelow, *Phys. Rev. Lett.* **102**, 030405 (2009).
 - [14] A. L. Fetter, *Rev. Mod. Phys.* **81**, 647 (2009).
 - [15] N. R. Cooper, *Adv. Phys.* **57**, 539 (2008).
 - [16] F. Dalfovo, S. Giorgini, M. Guilleumas, L. Pitaevskii, and S. Stringari, *Phys. Rev. A* **56**, 3840 (1997); E. Lundh, C. J. Pethick, and H. Smith, *ibid.* **58**, 4816 (1998).

- [17] S. Stringari, *Phys. Rev. Lett.* **86**, 4725 (2001); T.-L. Ho, *ibid.* **87**, 060403 (2001).
- [18] A. A. Penckwitt, R. J. Ballagh, and C. W. Gardiner, *Phys. Rev. Lett.* **89**, 260402 (2002); J.-P. Martikainen and H. T. C. Stoof, *ibid.* **91**, 240403 (2003).
- [19] G. Baym and C. J. Pethick, *Phys. Rev. A* **69**, 043619 (2004); J. A. M. Huhtamäki, M. Möttönen, and S. M. M. Virtanen, *ibid.* **74**, 063619 (2006).
- [20] A. Aftalion, X. Blanc, and J. Dalibard, *Phys. Rev. A* **71**, 023611 (2005); H. Pu, L. O. Baksmaty, S. Yi, and N. P. Bigelow, *Phys. Rev. Lett.* **94**, 190401 (2005).
- [21] H. Saito, Y. Kawaguchi, and M. Ueda, *Phys. Rev. Lett.* **102**, 230403 (2009); T. Mizushima and K. Machida, *Phys. Rev. A* **81**, 053605 (2010).
- [22] E. A. Ostrovskaya and Y. S. Kivshar, *Phys. Rev. Lett.* **93**, 160405 (2004); Y. V. Kartashov, B. A. Malomed, and L. Torner, *Phys. Rev. A* **75**, 061602(R) (2007).
- [23] F. Piazza, L. A. Collins, and A. Smerzi, *Phys. Rev. A* **80**, 021601(R) (2009).
- [24] R. P. Feynman, *Application of Quantum Mechanics to Liquid Helium*, Progress in Low Temperature Physics, Vol. I, edited by C. J. Gorter (North-Holland, Amsterdam, 1955).
- [25] M. Tsubota, K. Kasamatsu, and M. Ueda, *Phys. Rev. A* **65**, 023603 (2002); K. Kasamatsu, M. Tsubota, and M. Ueda, *ibid.* **67**, 033610 (2003).
- [26] D. L. Feder and C. W. Clark, *Phys. Rev. Lett.* **87**, 190401 (2001).
- [27] A. Barone and G. Paternò, *Physics and Applications of the Josephson Effect* (Wiley, New York, 1982).
- [28] V. M. Kurov and A. B. Kuklov, *Phys. Rev. A* **71**, 011601(R) (2005); **73**, 013627 (2006).
- [29] J. Brand, T. J. Haigh, and U. Zülicke, *Phys. Rev. A* **80**, 011602(R) (2009).
- [30] B. Wu and Q. Niu, *New J. Phys.* **5**, 104 (2003).
- [31] M. Liu, L. H. Wen, H. W. Xiong, and M. S. Zhan, *Phys. Rev. A* **73**, 063620 (2006).
- [32] L. H. Wen, J. S. Wang, J. Feng, and H. Q. Hu, *J. Phys. B* **41**, 135301 (2008).
- [33] S. Choi, S. A. Morgan, and K. Burnett, *Phys. Rev. A* **57**, 4057 (1998).
- [34] A. Aftalion and P. Mason, *Phys. Rev. A* **81**, 023607 (2010).
- [35] R. Carretero-Gonzalez, N. Whitaker, P. G. Kevrekidis, and D. J. Frantzeskakis, *Phys. Rev. A* **77**, 023605 (2008).
- [36] U. R. Fischer and G. Baym, *Phys. Rev. Lett.* **90**, 140402 (2003); G. M. Kavoulakis and G. Baym, *New J. Phys.* **5**, 51 (2003).